Nanoscale

PAPER

View Article Online
View Journal | View Issue

Cite this: *Nanoscale*, 2015, **7**, 1956

The functionalization of nanodiamonds (*diamondoids*) as a key parameter of their easily controlled self-assembly in micro- and nanocrystals from the vapor phase†

Maria A. Gunawan,[a,b] Didier Poinsot,[a] Bruno Domenichini,[c] Céline Dirand,[c] Sébastien Chevalier,[c] Andrey A. Fokin,[b,d] Peter R. Schreiner*[b] and Jean-Cyrille Hierso*[a,e]

Received 3rd August 2014,
Accepted 7th December 2014

DOI: 10.1039/c4nr04442h

www.rsc.org/nanoscale

We detail herein readily accessible processes to control previously unobserved robust self-assemblies of nanodiamonds (*diamondoids*) in micro- and nanocrystals from their mild vapor deposition. The chemical functionalization of uniform and discernible nanodiamonds was found to be a key parameter, and depending on the type of functional group (hydroxy, fluorine, *etc*.) and its position on the diamondoid, the structure of the discrete deposits can vary dramatically. Thus, well-defined anisotropic structures such as rod, needle, triangle or truncated octahedron shapes can be obtained, and self-assembled edifices of sizes ranging from 20 nm to several hundred micrometers formed with conservation of a similar structure for a given diamondoid. Key thermodynamic data including sublimation enthalpy of diamondoid derivatives are reported, and the SEM of the self-assemblies coupled with EDX analyses and XRD attest the nature and purity of nanodiamond crystal deposits. This attractive method is simple and outperforms in terms of deposit quality dip-coating methods we used. This vapor phase deposition approach is expected to allow for an easy formation of diamondoid nanoobjects on different types of substrates.

Introduction

Diamondoids are cage hydrocarbon molecules that can be described as fully hydrogen-terminated nanometer-sized diamonds.[1,2] Adamantane (**1**) and diamantane (**2**) are the smallest diamondoids and their selective functionalization can be achieved with high efficiency at various positions of the hydrocarbon cage (Fig. 1).[1] Ultra-disperse detonation nanodiamond[3–6] and diamondoids (also called *nanodiamonds*[7]) have shown impressive success in the utilization of diamond properties in various areas that span the fields of nanomedicine,[8–10] nanodevices for energy,[11a] and molecular machines.[12,13] For instance, large area self-assembled monolayers of thiolated diamondoids on gold surfaces exhibit intense monochromatic photoemission with an energy distribution width <0.5 eV, which is related to the negative electron affinity of the surface-attached nanodiamonds.[11]

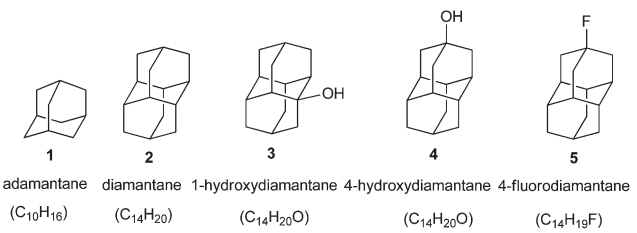

Fig. 1 Fully hydrogenated hydrocarbon cages adamantane **1** and diamantane **2**, and functionalized diamantane analogues **3–5**.

Another attractive and hitherto unmet challenge in this field is the construction of organic materials and organohybrids based on nano- and microcrystals of functionalized diamondoids. Based on such edifices, carbon nucleation followed by growth may also pave the way to access continuous

[a]*Institut de Chimie Moléculaire de l'Université de Bourgogne (ICMUB), UMR-CNRS 6302, Université de Bourgogne, 9 avenue Alain Savary, 21078 Dijon Cedex, France. E-mail: hiersojc@u-bourgogne.fr*
[b]*Institut für Organische Chemie, Justus-Liebig-Universität, Heinrich-Buff-Ring 58, 35392 Giessen, Germany. E-mail: prs@uni-giessen.de*
[c]*Laboratoire Interdisciplinaire Carnot de Bourgogne (LICB), UMR-CNRS 6303, Université de Bourgogne, 9 avenue Alain Savary, 21078 Dijon Cedex, France*
[d]*Department of Organic Chemistry, Kiev Polytechnic Institute, Pr. Pobedy 37, 03056 Kiev, Ukraine*
[e]*Institut Universitaire de France (IUF), 103 Bd. Saint Michel, 75005 Paris Cedex 5, France*

†Electronic supplementary information (ESI) available: Full details of vapor pressure measurements, vapor deposition of functionalized diamondoids, apparatus (including PVD) and all characterization for all functionalized diamondoids self-assemblies investigated from vapor phases and solution dip-coating. See DOI: 10.1039/c4nr04442h

diamond thin films of better defined structure and surface.[14] Diamondoids may also serve as precursors in "bottom-up" strategies to build organohybrids,[15] and to devise diamond structures under conditions that are possibly milder than the chemical vapor deposition (CVD) conditions currently used for diamond growth.[16] Methods have been reported akin to CVD that yielded higher diamondoids (more than four carbon fused-cages) and even diamond from diamondoid seeds.[17]

However, for applications of nanodiamond-based materials built "bottom-up" there is still a need for better fundamental understanding and mastering of the conditions of nucleation, growth and self-assembly of diamondoid units.[18] Additionally, general interest in dispersed micro- and nanocrystals stems from the fact that their properties dramatically change with their size and shape,[19] and many applications from optical (plasmon absorption) to medical (transportation through biological barriers) illustrate this point. We thus report on readily accessible processes for the mild vapor deposition of functionalized diamondoids that provide robust self-assembly of nanodiamonds micro- and nanocrystals. Key thermodynamic data including sublimation enthalpy of several diamondoid derivatives are reported from a new measurement protocol at solid–vapor thermodynamic equilibrium state. Easily accessible processes for self-assembled edifices of sizes ranging from 20 nm to several hundred micrometers are reported with remarkable conservation of the general geometry for a given diamondoid, chemical analysis with microscopy ascertaining the full preservation of the nature of nanodiamonds.

Results and discussion

Due to the volatility of adamantane (**1**) and diamantane (**2**) (Fig. 1), we envisioned that vapor deposition of functionalized diamondoids might be a general and convenient access to nanocrystals, microcrystals, and thin films of carbon-based materials. The control of a given vapor deposition process entails knowledge of the partial pressure of the source under the experimental conditions. Accordingly, enthalpies of sublimation are critical thermodynamic properties of the condensed phase in relationship with vapor pressure. Therefore, our vapor deposition studies were first devoted to measuring sublimation enthalpies of pristine adamantane and diamantane for which different values have been reported.[20,21] Conversely, fundamental studies of the vapor pressure of functionalized diamondoids remain very limited.[21b] We found significant differences in the reported values for the enthalpies of sublimation (see ESI,† Table 1S), depending on the measurement and calculation methods. Mainly destructive calorimetric measurements had been conducted using total combustion of the diamondoids in a bomb calorimeter.[22] This prompted us to develop an alternative experimental method to measure the vapor pressure of functionalized diamondoids at the solid–vapor thermodynamic equilibrium state. In this process the diamondoids were brought into the sublimation regime in a chamber connected with a Pirani vacuum gauge at ±0.13 Pa (*i.e.* ±1 μmHg) and the pressure was continuously monitored until the equilibrium state was reached. The temperature dependence of the vapor pressure for the diamondoids **1–5** follows the Clausius–Clapeyron equations given in Table 1.

Table 1 Thermodynamic data for sublimation of **1–5**[a]

	Clausius–Clapeyron equations	ΔH^0 (kJ mol^{-1})	r^2
1	$\ln P = -7212.4/T + 26.869$	60.0 ± 5	0.9991
2	$\ln P = -11\,073/T + 37.172$	92.1 ± 5	0.9992
3	$\ln P = -12\,282/T + 39.589$	102.1 ± 5	0.9960
4	$\ln P = -13\,087/T + 42.196$	108.8 ± 5	0.9983
5	$\ln P = -11\,597/T + 38.335$	96.4 ± 5	0.9965

[a] Pressure in Pa, T in K (see ESI for measurement full details).

The enthalpies of sublimation obtained from these equations are ΔH^0 = 60.0 kJ mol^{-1} for **1**, 92.1 kJ mol^{-1} for **2**, 102.1 kJ mol^{-1} for **3**, 108.8 kJ mol^{-1} for **4**, and 96.4 kJ mol^{-1} for **5**, indicating the highest volatility for adamantane, and the lowest for hydroxydiamantane derivatives. The enthalpy of sublimation obtained for adamantane **1** following equilibrium state pressure measurements, ΔH^0 = 60.0 kJ mol^{-1} (14.3 kcal mol^{-1}), is consistent with the values previously reported (14.2 ± 0.3 kcal mol^{-1}).[21a] This was also the case for diamantane **2** measurements (ΔH^0 = 92.1 kJ mol^{-1}), with the values obtained using calorimetry bomb combustion,[21a] and gas-saturation temperature scanning (95.9 kJ mol^{-1}).[23] As expected, the fluorodiamantane **5** was found to be fairly volatile with a ΔH^0 = 96.4 kJ mol^{-1} approaching the one we found for pristine diamantane. Due to a noticeable hygroscopic behaviour of the hydroxydiamantanes a good reproducibility required cautiously dried finely divided pure hydroxydiamantane powders to exclude water traces. It was determined that 4-hydroxydiamantane **4** is significantly less volatile, ΔH^0 = 108.8 kJ mol^{-1}, than 1-hydroxydiamantane **3**, ΔH^0 = 102.1 kJ mol^{-1}.[24]

The vapor deposition of **1–5** was then conducted, under tuneable conditions of pressure and temperature, on silicon and mica substrates using a simple sublimation apparatus (see ESI†). The deposition experiments were conducted first under air or argon atmosphere 1.0 bar (10^5 Pa), and then either under static vacuum (initial pressure 5.3 mbar) or dynamic vacuum (5.3 mbar). Temperature conditions ranging between 50 and 110 °C were investigated. Higher sublimation temperatures favour a higher vapor supersaturation regime, which in turn favours effective nucleation in comparison with crystal growth. A good nucleation rate, in comparison with growth rate, then will quickly generate numerous small crystals of critical size that will no longer disappear and serve as "nutrients" for the growth of bigger crystals (Ostwald ripening).[25] Deposition times were varied between a few minutes to 16 h. The vapor deposition of a wide variety of functionalized diamondoids was conducted (see ESI†), including compounds **1–5** (Fig. 2).

Other functionalized adamantane and diamantane derivatives, such as the 1-aminoadamantane, 1-adamantyldiphenylphosphinite, 1-adamantyldiphenyl-thiophosphinite, 1-ethynyl-

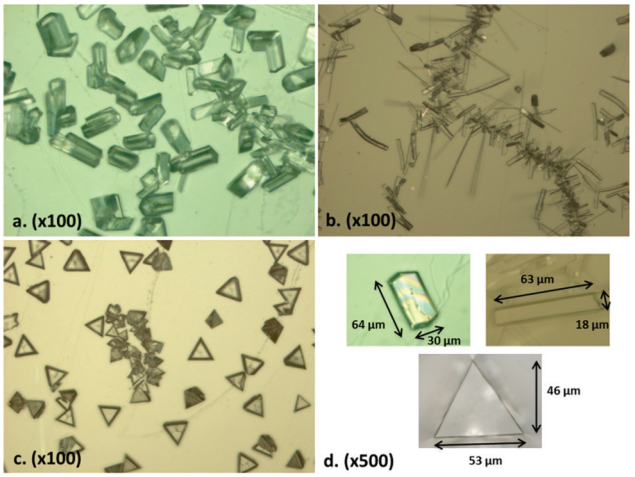

Fig. 2 Optical microscopy of deposits of functionalized diamantanes **3–5**. Deposition at 85 °C on mica for 30 min: (a) 1-hydroxydiamantane **3**; (b) 4-hydroxydiamantane **4**; (c) 4-fluorodiamantane **5**; (d) Enhancement from (a–c) micrographs of typical microcrystals of **3–5**.

adamantane, 1-hydroxyadamantane, 4,9-dihydroxydiamantane, 4,9-difluorodiamantane were also deposited (see details in ESI†). Optical microscopy of the deposits was conducted for visual inspection of the obtained deposits. Optimization of the deposition conditions was conducted for the diamondoids that were found most suitable for generating from vapor deposition well-defined crystals self-assembly. As illustrated in Fig. 2, crystals of a micrometer size with very different shapes and structures grew depending on the nature of the diamondoid. The deposition of **1** was difficult due to the high volatility of this compound which easily re-evaporates after condensation. The vapor deposition of **2**, although easier, resulted in very fragile assemblies that easily broke on handling (see microstructures in ESI†). Conversely, nice crystalline deposits of well-dispersed homogeneous microcrystals were obtained in less than one hour from the vapor deposition of hydroxyl- and fluoro-functionalized nanodiamonds **3–5**. Interestingly, not only the nature of the functionalization shows an overwhelming influence on the self-assembly and thus microstructure of the deposits, but also the position of the functional group on the cage. Thus, from the vapor deposition of **3–5**, hexagonal rod, rectangular needle, and triangular plate microcrystals were observed, respectively. The size of the crystals can be adjusted through the duration of the deposition with conservation of excellent dispersion and size homogeneity. The high crystallinity of the deposits was confirmed by successful single crystal X-ray diffraction analyses conducted on all these samples. For instance, the X-ray diffraction analysis of microcrystals of **3** (Fig. 17S in ESI†),[26] shows the presence of discrete tetramers for which the units are in a cyclic network of O–H···O hydrogen bonding. These tetramers are arranged in 1-D columns. A similar structure was found for **4**.

Scanning electron microscopy (SEM) analysis was conducted to examine surface morphologies in further details (Fig. 3). Much to our surprise the SEM images showed that the

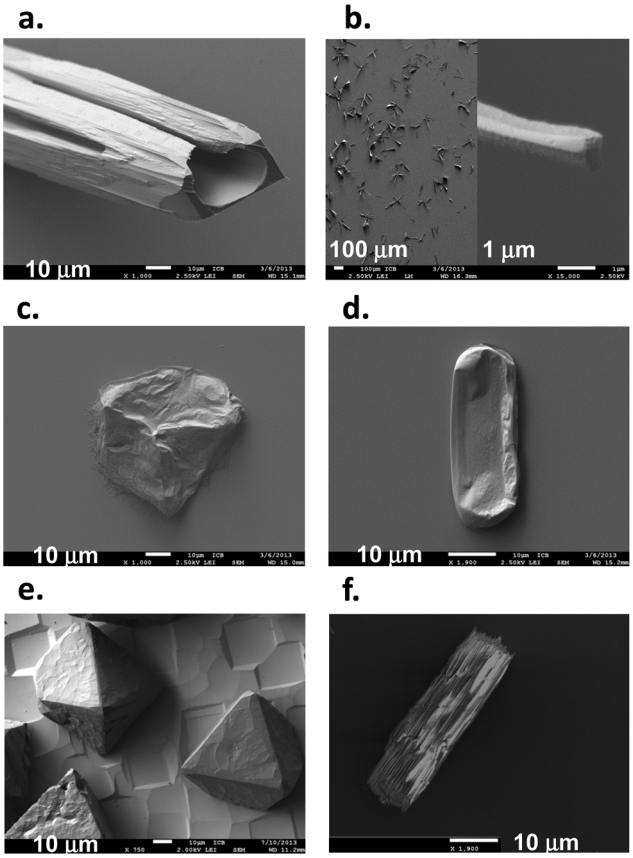

Fig. 3 SEM micrographs of self-assembled functionalized diamantanes deposited from the vapor phase: (a) hexagonal rod of **3** deposited at 1 bar (air or Ar); (b) needles of **4** deposited at 1 bar (air or Ar) protected by a gold layer before SEM analysis (enhancement of a hollow crystal, bottom right); (c) and (d) deposits of **5** and **3** protected by a gold layer before SEM analysis (as truncated octahedron and rod, respectively); (e) and (f) self-assembly of **5** and **3** deposited under 5.3 mbar dynamic vacuum.

first deposits elaborated under atmospheric pressure of air or argon do not tolerate the low pressure, 10^{-6} mbar, and the voltage imposed by SEM analysis. For instance, deposits of **5** were completely volatilized, and while self-assemblies of **3** and **4** were more resistant, they also showed a tendency toward shrinkage during the analysis. Microcrystals of **3** that appeared as well-defined hexagonal rods in optical microscopy turned into hollow rectangular structures under the SEM conditions (Fig. 3a). The formation of hollow needles for **4** is shown in the SEM micrographs (Fig. 3b) with shrinkage also evidenced for the needle crystals from collapsed edges shown in the enlarged picture (right). Hollow micro- and nanostructures are studied in areas which include catalysis, cosmetics, drug and gene delivery, hydrogen production and storage, photonics, photovoltaics, and rechargeable batteries.[27] Mostly metal-based and ceramic hollow micro-/nanostructures have been prepared, commonly from template-removing procedures. To the best of our knowledge, the formation of non-polymeric hollow structures of pure hydrocarbons has not previously

been documented. We hypothesized that their formation was either due to some unlikely selective internal volatilization and/or rearrangement of the self-assembly under the SEM conditions, or better to some gas capture –either air or argon– inside the structures during the growth process. To support the latter hypothesis, we tried to protect the diamondoid particles grown under atmospheric pressure by covering them with a 15–20 nm thin layer of gold metal before SEM analysis using sputtering by high resolution ion beam coater. This metallization was also achieved under high vacuum (10^{-5} mbar) and consequently the crystal morphologies were modified before the gold layer could fully protect the deposit. However, these experiments established that during the vapor deposition process under atmospheric pressure some gas was trapped inside the self-assembly of diamondoids. As shown in Fig. 3c and d respectively, shrinkage of the polyhedral particles based on triangle motifs for **5**, and hexagonal rods for **3** were observed, while the gold protective layer roughly conserved the original shape of the edifices.

With the goal of growing crystals in which no gas trapping occurs and that would also be resistant to the SEM conditions, we modified the vapor deposition apparatus used under atmospheric pressure to allow sublimation under 5 mbar reduced pressure (Fig. 16S in ESI†). We were delighted to confirm the success of this strategy. As illustrated in Fig. 3e and f, the deposition of microcrystals of about 40 μm was achieved, with the SEM revealing three-dimensional structures fully consistent with the optical microscopy observations. The triangular shapes observed in optical microscopy thus correspond to the faces of regular octahedra which result from the self-assembly from the vapor phase of fluorinated diamondoid **5**. The hexagonal rods observed for hydroxylated diamantane **3** revealed an apparent surface roughness that was not observed for **5**. EDX microanalysis conducted during the SEM experiments on various areas of the deposited samples confirmed elemental composition and nature of the deposits. This is illustrated in Fig. 4 that presents a deposit of **5** on silicon (area-Spect 3, EDX $C_{K\alpha1}$ = 0.280 keV, $F_{K\alpha1}$ = 0.532 keV) and compares it to a pristine zone of the silicon substrate (area-Spect 2, EDX $Si_{K\alpha1}$ = 1.739 keV). Thus, consistent with the single crystal X-ray diffraction analysis that attested high crystallinity and purity of the deposits, the peaks corresponding to the electron binding energies $K_{\alpha1}$ for C, F and Si were detected depending on the focus area of the beam. The size distribution in Fig. 4 confirmed an average size of 40 μm with the major part of the particles having a size between 25 and 55 μm. More than 90% of the visible aggregates have pyramidal and octahedral shapes, and less than 5% edifices experienced intense Ostwald ripening for reaching sizes above 60 μm.

Heavier plasma-hydrogenated detonation nanodiamond developed by Arnault and co-workers have shown a tendency to self-assembling as aggregates in water solution, depending on counter ions present.[28] Our attempts to generate accurate and reproducible self-assemblies such as obtained from vapor phases, but by crystallization from our functionalized diamondoids in solution (dip-coating, dichloromethane, water)

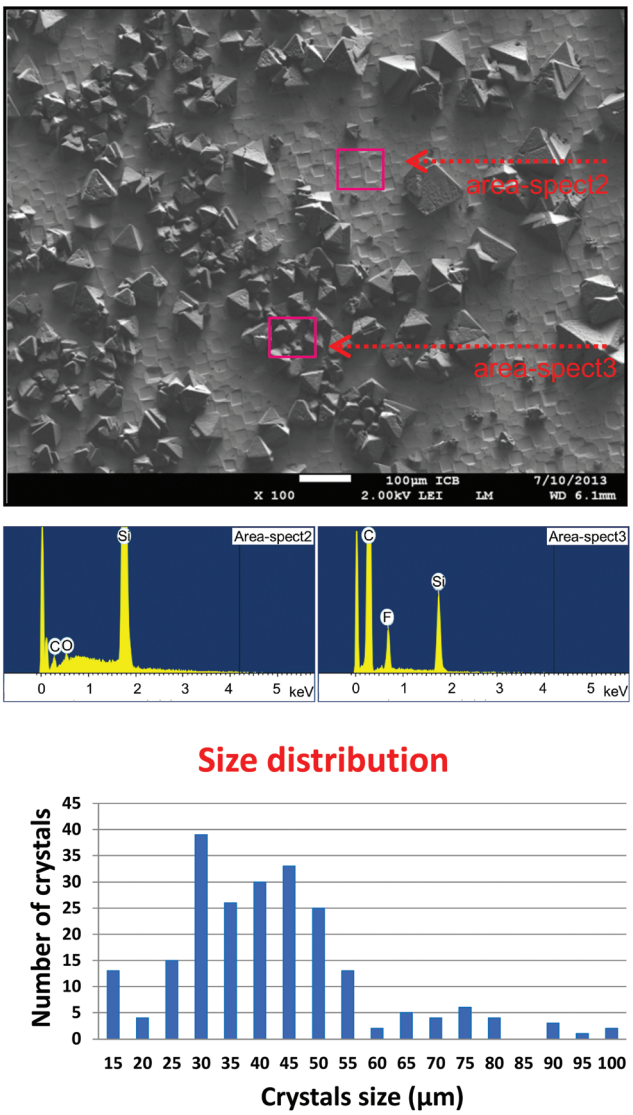

Fig. 4 SEM micrograph of **5** deposited on a silicon substrate (top). EDX analysis of different zones (area-Spect2 and area-Spect3), beam energy 5 keV, a beam size 1 μm^3. $C_{K\alpha1}$ = 0.280 keV, $F_{K\alpha1}$ = 0.532 keV and $Si_{K\alpha1}$ = 1.739 keV (middle). Related histogram of the size of crystals averaged at 40 ± 15 μm on >90% of particles (bottom).

were unsuccessful, giving mainly a large area covered with isotropic structurally poorly-defined coated material (see optical microscopy and SEM images in ESI†).

After having determined practical vapor deposition conditions for growing well-dispersed self-assembly of diamondoids as microcrystals – with various shapes depending on the diamondoid functionalization and on the position of the function on the cage – we addressed the more challenging task of growing crystals of nanometer size by a similar vapor deposition technique. A particularly pertinent issue was whether shapes and structures previously obtained from functionalized diamondoids vapor self-assembly would be conserved at the nanoscale. The very first step of deposition process could not be controlled by the simple evaporation apparatus we designed

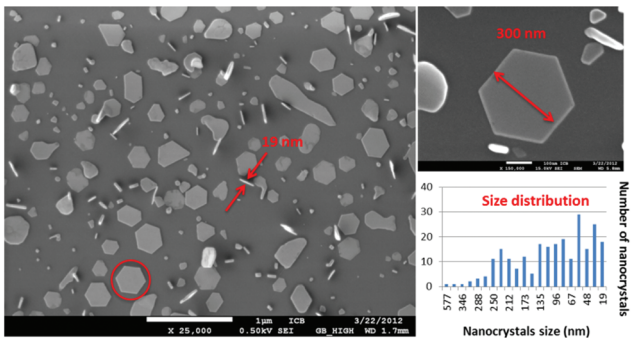

Fig. 5 SEM micrograph of nanocrystals of 1-hydroxydiamantane **3** deposited on Si(111)/SiO_2 by PVD under a pressure 1.4 × 10^{-6} mbar of argon (left). Magnification on a typical hexagonal-shaped nanocrystal (top right) and related histogram of the size of nanocrystals (bottom right).

for fast and easy self-assembly of diamondoids as microcrystals. Instead we thus used a three-chamber high vacuum physical vapor deposition (PVD, 10^{-9} mbar) apparatus incorporating *in situ* XPS analysis (see Fig. SXPS2 in ESI,† from **3** a typical C 1s peak at 284.0 eV appears). The vapor deposition of **3** under suitable vapor pressure was performed using this PVD apparatus, and led to the growth of well-defined crystalline hexagonal rods. Diamondoid vapours were brought very close to the substrates through a heating tube placed at 2 mm distance. Deposition on a silicon surface that was treated following a RCA protocol to remove carbon contamination was achieved from 20 mg of **3** heated at 100 °C for 3 h under a low pressure of 1.4 × 10^{-6} mbar. SEM images of the resulting deposits are provided in Fig. 5. As expected, these deposits were resistant to the SEM analysis conditions. Fig. 5 (bottom right) provides a representative histogram of the nanocrystals dispersion. Generally, sizes ranging between 20 and 600 nm were obtained under these conditions. Discrete 30–100 nm nanocrystals were obtained in majority (>70% of the particles). We were glad to observe that the self-assembly of **3** mostly exhibits hexagonal shapes with well-defined growth directions. These growth directions were not induced by the Si(111) substrate since an amorphous SiO_2 thin layer is always present at the surface of the substrate before deposition as confirmed by XPS (with O 1s peak of SiO_2 found at 532.5 eV, see Fig. SXPS1 in ESI†). Accordingly, owing to non-preferentially oriented macroscopic growth of nanocrystals some were positioned perpendicularly to the surface.

In the SEM picture Fig. 5 (left) these diamondoid particles can be easily identified and the images allowed measuring their thicknesses, which were remarkably regular around 20 nm. This regularity suggests a fairly homogeneous growth rate of the diamondoid particles. EDX analysis with a beam focusing on the edifices (beam energy 5 keV, size 1 μm^3) showed that the deposit of **3** exclusively contains carbon and oxygen, in full agreement with the chemical nature of the deposit (see Fig. SEDX1 in ESI†). We therefore demonstrated that particles of **3** of approximately 20 nm thickness and size can be deposited from a vapor phase under strictly anaerobic and low-pressure conditions (1.4 × 10^{-6} mbar), showing self-assembly into hexagonal structures similar to the microstructures formed at micrometer scale under few mbar pressure. This could be straightforwardly extended to the other nanodiamonds **4** and **5**.

The relation between the self-assemblies morphology and the functional groups in the molecular precursor is for now difficult to rationalize. This is related to the recognized general non-predictability of molecular structure and morphology of crystals. Accordingly, complexity in polymorphism of functionalized diamondoids has been recently illustrated for adamantane halide derivatives.[29] Nevertheless, it is worth mentioning the excellent reproducibility which is obtained from this approach in the formation of robust well-defined self-assemblies. This attractive method is very simple and in our case outperforms in terms of quality dip-coating popular methods (see ESI†). Accordingly, this mild temperature vapor phase deposition approach is expected to allow for an easy formation of diamondoid nanoobjects on different types of substrates, including sensitive ones.

Conclusions

In summary, we report here on readily accessible processes for the mild vapor deposition of functionalized nanodiamonds to provide previously unobserved self-assembly of organic micro- and nanocrystals. Key thermodynamic data including sublimation enthalpy of several diamondoid derivatives are reported from a new measurement protocol at solid–vapor thermodynamic equilibrium state. The conditions of pressure used for the depositions are crucial and if appropriately adjusted lead to deposits resistant to high vacuum and high energy beams. Vapor deposition under atmospheric pressure of air or argon led to unprecedented assemblies that apparently capture gases, and turn to hollow edifices upon gas evacuation. Finally, depending on the type of functional group and its position on the diamondoid, the general structure of the discrete deposits can vary dramatically and anisotropic structures such as rods, needles, triangles or in truncated octahedra form. Self-assembled edifices of sizes ranging from 20 nm to several hundred micrometers can be obtained with conservation of a similar geometry for a given diamondoid. Our ongoing work aims at using these diamondoid self-assemblies having reactive functions (OH, F) as supports and seeds for metal deposition and organohybrid diamond constructions.

Experimental

General

Pristine adamantane and diamantane were prepared and purified by sublimation before use.[2] 1-Aminoadamantane and 1-hydroxyadamantane were obtained from commercial sources. 1-Hydroxydiamantane, 4-hydroxydiamantane, and 4,9-

dihydroxydiamantane were synthesized from diamantane;[30] 4-fluorodiamantane and 4,9-difluorodiamantane were prepared from its hydroxyl derivatives.[31] Syntheses of other functionalized nanodiamonds were from literature reports. Full details of vapor pressure measurements, vapor deposition of functionalized diamondoids, apparatus, including PVD, and all characterization are described in the ESI.†

Mild controlled self-assembly of functionalized nanodiamonds from vapor phases. A functionalized diamondoid (**1**–**5**) was placed in a DSC cup on a boron nitride heating element. The substrate was placed above this DSC cup and separated by a ceramic spacer. The whole system was sealed using copper gasket and a valve that was connected to either vacuum line (5 mbar pressure), or argon (1 atm), or air (1 atm). With the vacuum line the inner gas was removed by pumping for 5 min, and then sublimation was started by adjusting the intensity of the current and duration of deposition. After adjusting the intensity of the applied current the deposition started. The temperature setting was also monitored as a function of time. After the deposition time, the source was switched off allowing the system to cool. Once the temperature dropped below 30 °C, the system was opened, the substrate on which the deposit was made was characterized by optical microscopy and by scanning electron microscopy (SEM), EDX and additionally by X-ray diffraction. To avoid tampering samples were stored sealed in a freezer at 4 °C.

Physical vapor deposition. Typically a Si(111) wafer 1×1 cm^2 was cleaned from carbon-based contamination with RCA clean (see ESI†) and kept inside the heating chamber of a PDV apparatus. An amorphous SiO_2 thin layer forms, the Si(111)/SiO_2 then were heated by induction at 800 °C for 12 min, and then moved into the main vacuum deposition chamber with an initial pressure of 1.6×10^{-8} mbar. A glass tube containing 1-hydroxydiamantane (**3**) was purged before the connection valve was opened and then heated with heating wire at around 80 °C for 3 h; the pressure increased to about 1.4×10^{-6} mbar. *In situ* XPS analysis allowed monitoring of the deposition process. After cooling, the sample was removed from the PVD apparatus, and to avoid its altering it was stored sealed in a freezer at 4 °C.

Acknowledgements

This work was supported by the "*Conseil Régional de Bourgogne*" (18 months PhD grant for M. A. G. in project PARI-IME SMT08) and by the CNRS through 3MIM P4-program on *nanodiamonds functionalization for biological applications*. The work in Giessen was in part supported by the Department of Energy, Office of Basic Energy Sciences, Division of Materials Science and Engineering, under contract DE-AC02-76SF00515. Thanks are due to Frederic Herbst (LICB, Dijon), Claire-Hélène Brachais (ICMUB, Dijon), and Philippe Richard (ICMUB, Dijon), for their assistance with EDX, DSC, and XRD measurements, respectively.

Notes and references

1 M. A. Gunawan, J.-C. Hierso, D. Poinsot, A. A. Fokin, N. A. Fokina, B. A. Tkachenko and P. R. Schreiner, *New J. Chem.*, 2014, **38**, 28.
2 H. Schwertfeger, A. Fokin and P. R. Schreiner, *Angew. Chem., Int. Ed.*, 2008, **47**, 1022.
3 V. N. Mochalin, O. Shenderova, D. Ho and Y. Gogotsi, *Nat. Nanotechnol.*, 2012, **7**, 11.
4 A. Krueger, *Adv. Mater.*, 2008, **20**, 2445.
5 *Ultrananocrystalline Diamond: Synthesis, Properties and Applications*, ed. O. Shenderova and D. Gruen, William-Andrew Publishing, Norwich, NY, USA, 2006.
6 A. Krueger and D. Lang, *Adv. Funct. Mater.*, 2012, **22**, 890.
7 We reserve "nanodiamond" as a generic name for mixtures of compounds (mostly originating from CVD or detonation methods), and in singular form because it is a class of materials. The term "nanodiamonds" used for diamondoids on the other hand implies, because of plural, that the individual entities can be counted, that is, they have to be uniform and discernible nanometer sized molecules.
8 L. Moore, E. K.-H. Chow, E. Osawa, J. M. Bishop and D. Ho, *Adv. Mater.*, 2013, **25**, 3532.
9 O. Faklaris, V. Joshi, T. Irinopoulou, P. Tauc, M. Sennour, H. Girard, C. Gesset, J.-C. Arnault, A. Thorel, J. P. Boudou, P. A. Curmi and F. Treussart, *ACS Nano.*, 2009, **3**, 3955.
10 A. Krueger, *Chem. – Eur. J.*, 2008, **14**, 1382.
11 (*a*) W. L. Yang, J. D. Fabbri, T. M. Willey, J. R. I. Lee, J. E. Dahl, R. M. K. Carlson, P. R. Schreiner, A. A. Fokin, B. A. Tkachenko, N. A. Fokina, W. Meevasana, N. Mannella, K. Tanaka, X. J. Zhou, T. van Buuren, M. A. Kelly, Z. Hussain, N. A. Melosh and Z.-X. Shen, *Science*, 2007, **316**, 1460; (*b*) W. A. Clay, Z. Liu, W. Yang, J. D. Fabbri, J. E. Dahl, R. M. K. Carlson, Y. Sun, P. R. Schreiner, A. A. Fokin, B. A. Tkachenko, N. A. Fokina, P. A. Pianetta, N. Melosh and Z. X. Shen, *Nano Lett.*, 2009, **9**, 57.
12 P.-L. E. Chu, L. Y. Wang, S. Khatua, A. B. Kolomeisky, S. Link and J. M. Tour, *ACS Nano.*, 2013, **7**, 35.
13 S. D. Karlen, R. Ortiz, O. L. Chapman and M. A. Garcia-Garibay, *J. Am. Chem. Soc.*, 2005, **127**, 6554.
14 Y.-C. Chen and L. Chang, *RSC Adv.*, 2014, **4**, 18945.
15 Few diamondoid-based hybrid compounds exist, see for cluster and MOOFs species: (*a*) A. B. Lysenko, G. A. Senchyk, J. Lincke, D. Lassig, A. A. Fokin, E. D. Butova, P. R. Schreiner, H. Krautscheid and K. V. Domasevitch, *Dalton Trans.*, 2010, **39**, 4223; (*b*) B. E. K. Barth, B. A. Tkachenko, J. P. Eußner, P. R. Schreiner and S. Dehnen, *Organometallics*, 2014, **33**, 1678.
16 *Physics and Applications of CVD Diamond*, ed. S. Koizumi, C. Nebel and M. Nesladek, Wiley-VCH, Weinheim, Germany 2008, pp. 13–93.
17 J. E. P. Dahl, J. M. Moldovan, Z. Wei, P. A. Lipton, P. Denisevich, R. Gatt, S.-G. Liu, P. R. Schreiner and R. M. K. Carlson, *Angew. Chem., Int. Ed.*, 2010, **49**, 9881.

18 J.-C. Arnault and H. A. Girard, in *Nanodiamond, Diamond Nucleation and Seeding Techniques*, ed. O. A. Williams, RSC, Cambridge, 2014, pp. 221–252.
19 C. Burda, X. Chen, R. Narayanan and M. A. El-Sayed, *Chem. Rev.*, 2005, **105**, 1025.
20 J. S. Chickos and W. E. Acree Jr., *J. Phys. Chem. Ref. Data*, 2002, **31**, 537.
21 (*a*) T. Clark, T. Knox, H. Mackle, M. A. McKervey, H. Mackle and J. J. Rooney, *J. Am. Chem. Soc.*, 1979, **101**, 2404; (*b*) T. Clark, T. Knox, M. A. McKervey and H. Mackle, *J. Chem. Soc., Perkin Trans. 2*, 1980, 1686.
22 Concerning diamantane, enthalpy of sublimation ΔH^0 = 117.2 ± 8 kJ mol^{-1} was reported (see ref. 18) that was calculated from the sum of the enthalpy of vaporization and the enthalpy of fusion, see: A. S. Carson, P. G. Laye, W. V. Steele, D. E. Johnston and M. A. McKervey, *J. Chem. Thermodyn.*, 1971, **3**, 915. Various other methods have been used which conversely gave for diamantane ΔH^0 values ranging between 73 and 97 kJ mol^{-1} (see also ESI†).
23 T. Clark, T. Knox, H. Mackle, M. A. McKervey and J. J. Rooney, *J. Chem. Soc., Perkin Trans. 1*, 1975, **71**, 2107.
24 The identical sublimation enthalpy values reported at 116–118 kJ mol^{-1} for diamantan-1-ol, diamantan-3-ol and diamantan-4-ol are questionable and may be overestimated according our measurements (see ref. 21). Accordingly, DSC measurements of the melting points for **3** and **4** also showed ΔH discrepancies with values substantially different for 1-hydroxydiamantane and 4-hydroxydiamantane: 137 ± 1 °C and 177 ± 1 °C, respectively. DSC measurements on cooling were also achieved for determining crystallization peaks that gave single peak excluding polymorphism of **3** and **4** between 25 and 210 °C.
25 (*a*) J.-C. Hierso, R. Feurer and P. Kalck, *Chem. Mater.*, 2000, **12**, 390; (*b*) P. Serp, J.-C. Hierso and P. Kalck, in *Topics in Organometallic Chemistry: Precursor Chemistry of Advanced Materials: CVD, ALD and Nanoparticles*, 2005, vol. 9, pp. 147–171; (*c*) J.-C. Hierso, C. Satto, R. Feurer and P. Kalck, *Chem. Mater.*, 1996, **8**, 2481.
26 C. Y. Yu, Q. Li, L. B. Wang and H. W. Ma, *Acta Crystallogr., Sect. E: Struct. Rep. Online*, 2006, **62**, o2369.
27 (*a*) X. W. Lou, L. A. Archer and Z. Yang, *Adv. Mater.*, 2008, **20**, 3987; (*b*) X. W. Lou, Y. Wang, C. Yuan, J. Y. Lee and L. A. Archer, *Adv. Mater.*, 2006, **18**, 2325; (*c*) H. J. Hah, J. S. Kim, B. J. Jeon, S. M. Koo and Y. E. Lee, *Chem. Commun.*, 2003, 1712; (*d*) Y. Sun, B. Mayers and Y. Xia, *Adv. Mater.*, 2003, **15**, 641.
28 T. Petit, H. A. Girard, A. Trouvé, I. Batonneau-Gener, P. Bergonzo and J.-C. Arnault, *Nanoscale*, 2013, **5**, 8958.
29 P. Negrier, M. Barrio, J. L. Tamarit and D. Mondieig, *J. Phys. Chem. B.*, 2014, **118**, 9595 and references therein.
30 N. A. Fokina, B. A. Tkachenko, A. Merz, M. Serafin, J. E. P. Dahl, R. M. K. Carlson, A. A. Fokin and P. R. Schreiner, *Eur. J. Org. Chem.*, 2007, 4738.
31 H. Schwertfeger, C. Würtele, H. Hausmann, J. E. P. Dahl, R. M. K. Carlson, A. A. Fokin and P. R. Schreiner, *Adv. Synth. Catal.*, 2009, **351**, 1041.